The Astrophysical Journal, 663:139–149, 2007 July 1

ACCURATE REALIZATIONS OF THE IONIZED GAS IN GALAXY CLUSTERS: CALIBRATING FEEDBACK

Paul Bode and Jeremiah P. Ostriker
Department of Astrophysical Sciences, Peyton Hall, Princeton University, Princeton, NJ 08544; bode@astro.princeton.edu, ostriker@princeton.edu

Jochen Weller
University College London, Gower Street, London WC1E 6BT, UK; jochen.weller@ucl.ac.uk

and

Laurie Shaw
Department of Physics, McGill University, Montreal, QC H3A 2T8, Canada; lds@hep.physics.mcgill.ca
Received 2006 December 21; accepted 2007 March 23

ABSTRACT

Using the full, three-dimensional potential of galaxy cluster halos (drawn from an *N*-body simulation of the current, most favored cosmology), the distribution of the X-ray–emitting gas is found by assuming a polytropic equation of state and hydrostatic equilibrium with constraints from conservation of energy and pressure balance at the cluster boundary. The resulting properties of the gas for these simulated redshift zero clusters (the temperature distribution, mass-temperature and luminosity-temperature relations, and the gas fraction) are compared with observations in the X-ray of nearby clusters. The observed properties are reproduced only under the assumption that substantial energy injection from nongravitational sources has occurred. Our model does not specify the source, but star formation and active galactic nuclei (AGNs) may be capable of providing this energy, which amounts to $(3–5) \times 10^{-5}$ of the rest mass in stars (assuming 10% of the gas initially in the cluster forms stars). With the method described here, it is possible to generate realistic X-ray and Sunyaev-Zel'dovich cluster maps and catalogs from *N*-body simulations with the distributions of internal halo properties (and their trends with mass, location, and time) taken into account.

Subject headings: cosmology: theory — galaxies: clusters: general — intergalactic medium — X-rays: galaxies: clusters

Online material: color figures

1. INTRODUCTION

Current and upcoming surveys in a variety of wavelength bands will increase the number of well-observed clusters of galaxies by at least an order of magnitude, while probing to much higher redshifts than before. Understanding the physical state of the intracluster medium (ICM) will be essential to exploiting this new data. In particular, it is necessary to develop methods of accurately modeling the thermal state of the gas in clusters before one can extract cosmological information from large surveys, which measure quantities arising from that state. For cluster-sized halos in a cosmological setting, the theoretical final distribution expected from the gravitational collapse of the dark matter (DM) is well understood (Navarro et al. 1997, 2004; Bullock et al. 2001; Jing & Suto 2002; Power et al. 2003; Zhao et al. 2003; Tasitsiomi et al. 2004; Reed et al. 2005b; Bartelmann et al. 2005; Diemand et al. 2005; Shaw et al. 2006; Lu et al. 2006). Measurements of the DM density profile in galaxy groups and clusters agree well with this theoretical expectation (Lewis et al. 2003; Dahle et al. 2003; Pratt & Arnaud 2005; Pointecouteau et al. 2005; Comerford et al. 2006; Łokas et al. 2006; Rines & Diaferio 2006; Zekser et al. 2006; Mandelbaum et al. 2006; Gastaldello et al. 2006; Schmidt & Allen 2006; Saha et al. 2006). However, the hot intracluster gas in these systems does not parallel the DM in either density or temperature distribution.

Much progress has been made in understanding the expected ICM distribution inside a standard DM halo (with the density profile showing a power-law cusp as in Navarro et al. [1997], Moore et al. [1999], or similar papers). Makino et al. (1998) gave an analytic expression for the density of isothermal gas in hydrostatic equilibrium with a Navarro-Frenk-White (NFW) potential; this was soon extended to nonisothermal gas with a polytropic equation of state (Suto et al. 1998; Wu et al. 2000; Loewenstein 2000; Ascasibar et al. 2003), and to triaxial halos (Lee & Suto 2003; Wang & Fan 2006). The resulting gas profiles possess a finite density core, not a cusp as seen in the DM.

The gross energetics of the gas do not parallel that of the DM either. Assuming that the gas energy comes solely from gravitational collapse gives the self-similar scalings between mass M, luminosity L, and temperature T of $M \propto T^{3/2}$ and $L \propto T^2$ (Kaiser 1986; Eke et al. 1998). However, these scalings do not agree with the observed relations, leading Kaiser (1991) to propose that nongravitational energy injection is important. This idea has gained support from a number of analytic investigations into polytropic ICM in DM potentials (Balogh et al. 1999; Suto et al. 1998; Wu et al. 2000; Loewenstein 2000; Tozzi & Norman 2001; Komatsu & Seljak 2001; Babul et al. 2002; Voit et al. 2002; Dos Santos & Doré 2002; Shimizu et al. 2004; Lapi et al. 2005; Afshordi et al. 2005; Solanes et al. 2005). An additional departure from self-similarity can come from star formation, which selectively removes gas with short cooling times, low entropy, and low total energy, leaving behind higher entropy material (Voit & Bryan 2001; Tozzi & Norman 2001; Voit et al. 2002; Scannapieco & Oh 2004). Detailed computer simulations

including star formation and feedback are confirming the importance of nongravitational processes (e.g., Borgani et al. 2005; Ettori et al. 2006; Sijacki & Springel 2006; Borgani et al. 2006; Romeo et al. 2006; Muanwong et al. 2006; Nagai 2006 and references therein). It appears from the cited papers that both processes are at work; low-entropy gas is incorporated into stars, and energy and metals are added to the remaining gas via feedback processes.

Based on these advances in our understanding of clusters, one can usefully combine prescriptions for gas physics with analytic modeling of DM profiles, but this method has limitations. Since halos are formed by stochastic merging of subunits, there is true scatter in halo concentration and inner slope (Avila-Reese et al. 1999; Jing 2000; Subramanian et al. 2000; Bullock et al. 2001; Klypin et al. 2001; Faltenbacher et al. 2005), which can vary with time and halo mass (Wechsler et al. 2002; Ricotti 2003; Zhao et al. 2003; Tasitsiomi et al. 2004; Salvador-Solé et al. 2005; Shaw et al. 2006; Wechsler et al. 2006). Similar variations exist in halo triaxiality (e.g., Kasun & Evrard 2005; Allgood et al. 2006; Ho et al. 2006; Rahman et al. 2006 and references therein) and substructure (e.g., Gill et al. 2004; Reed et al. 2005a; Shaw et al. 2006 and references therein). The clustering of halos has been shown to depend on age or concentration, as well as mass (Berlind et al. 2006 and references therein). Thus, mass, environment, and formation history all play significant roles in determining halo properties.

In prior work, Ostriker et al. (2005) improved on the use of analytic DM potentials by instead using the full three-dimensional potential of halos drawn from *N*-body simulations, combining these detailed three-dimensional models with current modeling of the gas physics. This procedure has the advantage of including the full distribution of halo concentration, as well as halo triaxiality and substructure. By drawing on a large *N*-body simulation volume (computationally much less costly than a full hydrodynamic run), trends of internal halo properties with mass, location, and time are all included, along with halo-halo correlations. This procedure inevitably requires the use of certain dimensionless parameters which, since they derive from feedback processes, are difficult, at present, to determine from ab initio computations. The purpose of the present paper is to tie down these parameters using observations of X-ray clusters. In particular, we apply the method of Ostriker et al. (2005) to a set of halos drawn from a large DM simulation of a cosmology in accord with the *Wilkinson Microwave Anisotropy Probe* (*WMAP*) 3 year data (Spergel et al. 2007). The resulting catalog is compared to X-ray observations of nearby clusters. The amount of energy input from nongravitational sources can significantly affect gas properties, but with the proper amount, consistent with AGN activity, this method can reproduce the properties of the local cluster population.

The procedures used to create the simulated cluster sample are described in § 2, these clusters are compared to X-ray observations in § 3, and we discuss the implications in § 4. One extension of this work is to use the gas properties to compute the Sunyaev-Zel'dovich (SZ) effect; Sehgal et al. (2007) do this to make available simulated large-area, subarcminute resolution microwave sky maps.

2. THE SIMULATED CLUSTER CATALOG

2.1. *Dark Matter Halos*

To produce a population of DM halos, we chose cosmological parameters to match the results from the *WMAP* 3 year data combined with large-scale structure observations (Spergel et al. 2007). The spatially flat ΛCDM model was used with total matter density $\Omega_m = 0.26$, baryon density $\Omega_b = 0.044$ (so the cosmic mean baryon fraction $f_c \approx 0.169$), and cosmological constant $\Omega_\Lambda = 0.74$. In addition, the Hubble constant $H_0 = 72\ \mathrm{km\ s^{-1}\ Mpc^{-1}}$ (i.e., $h = 0.72 = H_0/100\ \mathrm{km\ s^{-1}\ Mpc^{-1}}$), the primordial scalar spectral index $n_s = 0.95$, and the linear matter power spectrum amplitude $\sigma_8 = 0.77$. Concerning the *N*-body simulation parameters, the number of particles $N = 1024^3$ and the box size $L = 1000\ h^{-1}$ Mpc, making the particle mass $m_p = 6.72 \times 10^{10}\ h^{-1}\ M_\odot$; the cubic spline (see Hernquist & Katz 1989) softening length $\epsilon = 16.3\ h^{-1}$ kpc. The initial conditions for the *N*-body run were created with the GRAFIC1 code[1] (Bertschinger 2001) with a few modifications. Because the spherical Hanning filter employed in this code to isotropize small-scale structure also significantly suppresses power on small scales, it was not used. The linear DM transfer function at $z = 0$ was calculated with the CMBFAST (Zaldarriaga & Seljak 2000) code.[2] The DM growth factor was used to scale the resulting power spectrum to the initial simulation redshift, chosen to be when the density fluctuation amplitude on the grid scale is 10%, $z = 35.3$. With these parameters, a cluster with mass $\sim 7 \times 10^{14}\ h^{-1}\ M_\odot$ would contain 10^4 particles; a typical core radius for such a cluster would be $\sim 250\ h^{-1}$ kpc, or 15 times the particle softening length.

The simulation was run with the TPM code[3] (Bode et al. 2000; Bode & Ostriker 2003) with a couple of improvements over the publicly released version. Most variables in the improved code are double precision (including particle positions and velocities) with the main exception of accelerations and potentials, which are still single precision. In addition, no lower limit was set to the parameter *B* used in the TPM domain decomposition (see eq. [5] of Bode & Ostriker 2003). This means that at late times, there will be more particles followed at full force resolution, leading to improved simulation of the lowest mass objects; at $z = 0$ all cells with eight or more particles were followed with trees. The initial domain decomposition parameters were $A = 1.9$ and $B = 9.2$, the PM mesh contained 2048^3 cells, and the maximum subbox size was 256 cells. At the end of the run, 54% of the particles contained in 2% of the total volume were being followed with 5×10^6 trees.

The standard friends-of-friends (FOF) halo finder with linking length $b = 0.2$ was run on the simulation volume at $z = 0$, identifying almost 2×10^6 halos with 30 or more particles. The resulting mass function agrees well with the fitting formula of Warren et al. (2006); the difference in the cumulative mass function is less than 5% over the range $2 \times 10^{12} \leq M_{\mathrm{fof}}/(1\ h^{-1}\ M_\odot) \leq 10^{14}$ and less than 15% above this. In what follows, only halos containing gas with temperatures above 1.5 keV will be included in our discussion. We find only halos with $M_{500} > 10^{13}\ h^{-1}\ M_\odot$ will ever meet this limit (although it typically takes over twice this mass); $10^{13}\ h^{-1}\ M_\odot$ corresponds to 150 particles, so the question arises as to whether or not there is sufficient numerical resolution for such halos. To test this, we compared the halos described in this paper with a sample taken from a higher resolution *N*-body simulation. This high-resolution run has a box size $L = 320\ h^{-1}$ Mpc and a spline softening length $\epsilon = 3.2\ h^{-1}$ kpc, so the mass resolution is thus improved by a factor of 30 and the spatial resolution by a factor of 5; otherwise it was generated and evolved in exactly the same manner as the simulation described above. When applying the gas prescription of § 2.2, we

[1] This code is available at http://web.mit.edu/edbert/.
[2] Available at http://www.cmbfast.org/.
[3] Available at http://www.astro.princeton.edu/~bode/TPM/.

TABLE 1
Test of Resolution for Low-Mass Halos

Parameter	$1 < M_{500} \leq 4$		$4 < M_{500} \leq 6$	
	Standard	High Res.	Standard	High Res.
M_{500} ($10^{13}\ h^{-1}\ M_\odot$)	3.18 ± 0.55	3.29 ± 0.51	4.85 ± 0.57	4.81 ± 0.56
$kT_{\rm ew}$ (keV)	1.68 ± 0.19	1.75 ± 0.21	1.99 ± 0.24	1.97 ± 0.21
$L_{\rm X}$ ($10^{42}\ h^{-2}$ ergs s^{-1})	1.14 ± 0.76	1.21 ± 1.02	3.63 ± 1.99	3.79 ± 2.77
$L_{\rm SZ}$ ($10^{12}\ h^{-1}$ keV $M_\odot$)	3.31 ± 1.95	3.16 ± 1.95	7.13 ± 3.91	6.24 ± 2.94

Note.—Values are the mean and 1 standard deviation.

used a mesh cell size of $l = 9.60\ h^{-1}$ kpc, a factor of 3.4 smaller than the standard case (it was difficult to go to any finer mesh because of the memory requirements of the resulting large computational arrays). The maximum-feedback model (described below) was assumed. Table 1 compares the mean and standard deviation for several observables predicted in the standard and high-resolution runs, using two mass bins corresponding roughly to temperatures of 1.7 and 2 keV; little difference is evident. A smaller cell size leads to a smaller volume around each halo (for the same number of cells); this accounts for most of the differences seen in the two samples. The mass resolution is relatively unimportant. Increasing the cell size to $l = 12.80\ h^{-1}$ kpc in the high-resolution run results in a distribution even closer to the standard run.

2.2. *The Gas Prescription*

The gas distribution in each halo is calculated according to the prescription of Ostriker et al. (2005). Gas is placed in hydrostatic equilibrium with the DM gravitational potential of the halo using a polytropic equation of state. Pressure balance with infalling gas near the virial radius and energy conservation determine the two constants required for the polytropic fit. Two important processes alter the gas energy. Star formation removes low-entropy gas; we fix the conversion of gas into stars at 10%. This leaves the most important free parameter, which is the energy input into the cluster gas via feedback processes. We will show that with a reasonable amount of feedback it is possible to match X-ray observations of hot cluster gas.

In detail, a cubic mesh enclosing the particles is placed around the halo with the cell size twice the particle spline softening length, or $l = 32.55\ h^{-1}$ kpc. The mass m_p for each particle is placed on the mesh using the cloud-in-cell method, yielding the DM density, ρ_{Dk}, for each cell k. The gravitational potential on the mesh, ϕ_k, is computed from the density as in a standard particle-mesh code, but with a nonperiodic fast Fourier transform (FFT). The center of the cluster is defined as the cell with the lowest potential, $\phi_0 = \min(\phi_k)$. The radii enclosing various overdensities are calculated at this point, the outermost being the virial radius, $r_{\rm vir}$, enclosing the overdensity expected from spherical top-hat collapse, or 97 times the critical density at $z = 0$ for the cosmology used here (this is a change from Ostriker et al. [2005], where overdensity 200 was used). The velocity of the cluster as a whole is taken to be the mean velocity of the 125 particles closest to the cluster center (or, for halos with fewer than 250 particles, the innermost half). Particle velocities are moved to the rest frame of the cluster, and then the kinetic energy (KE) of each particle is placed on the grid in the same manner as the mass, yielding the KE per unit volume $\frac{1}{2}t_{Dk}$.

It is assumed that gas originally had the same distribution as the DM with density $f_c\rho_{Dk}$ and KE $f_c\frac{1}{2}t_{Dk}$ ($f_c \equiv \Omega_b/\Omega_m$). A certain amount of the gas mass, $M_\star$ (described below), will have turned into stars; this is presumably the most bound material, so cells are ranked by binding energy $\phi_k + \frac{1}{2}t_{Dk}$, and then cells are checked off until the sum of the masses $f_c\rho_{Dk}l^3$ equals $M_\star$. The initial mass M_g and energy E_g of the remaining gas are thus

$$M_g = \sum_k f_c\rho_{Dk}l^3, \tag{1}$$

$$E_g = \sum_k f_c\left(\phi_k\rho_{Dk} + \frac{1}{2}t_{Dk}\right)l^3, \tag{2}$$

where the sum is over all cells inside $r_{\rm vir}$ except those marked off for star formation. In addition, the gas surface pressure P_s on the cluster exerted by surrounding material is estimated from the KE in a buffer region nine cells ($293\ h^{-1}$ kpc) thick outside of $r_{\rm vir}$,

$$P_s = N_b^{-1}\sum_{k=1}^{N_b}\frac{f_c}{3}t_{Dk}, \tag{3}$$

where the sum is over the N_b cells in the buffer region $r_{\rm vir} < r_k < r_{\rm vir} + 9l$.

Now suppose the gas is allowed to rearrange itself within the DM potential such that it is in hydrostatic equilibrium and has a polytropic equation of state with index $\Gamma = 1.2$. There is much support for such a model; see the discussion and Figure 1 in Ostriker et al. (2005) comparing the polytropic model with a full, high-resolution cosmological simulation by G. Bryan; see also Ascasibar et al. (2006). We will treat the gas as a tracer such that the potential, set by the DM, does not change. Defining

$$\theta_k \equiv 1 + \frac{\Gamma - 1}{(1 + \delta_{\rm rel})\Gamma}\frac{\rho_0}{P_0}(\phi_0 - \phi_k), \tag{4}$$

as in Ostriker et al. (2005), the resulting gas pressure P and density ρ are given by

$$P(\boldsymbol{r}_k) = P_0\theta_k^{\Gamma/(\Gamma-1)}, \tag{5a}$$

$$\rho(\boldsymbol{r}_k) = \rho_0\theta_k^{\Gamma/(\Gamma-1)}, \tag{5b}$$

where $\delta_{\rm rel}$ is a nonthermal component of pressure, assumed to be proportional to thermal pressure such that the total $P_{\rm tot} = (1 + \delta_{\rm rel})P$. To specify the final gas distribution given these assumptions, two quantities still need to be determined, namely, the pressure P_0 and density ρ_0 at the potential minimum. This can be done with two equations of constraint, derived by requiring conservation of energy and by matching the external surface pressure, as follows. For a given choice of P_0 and ρ_0, the final radius r_f of

the gas initially inside $r_{\rm vir}$ can be found by summing outward from the cluster center until the initial mass M_g is enclosed,

$$\sum_{r_k<r_f} \rho_0 \theta_k^{1/(\Gamma-1)} l^3 = M_g. \quad (6)$$

This implies that gas may expand or contract, changing the gas fraction inside $r_{\rm vir}$. Assuming the external surface pressure changes little with radius, there will be mechanical work done, causing a change in energy proportional to the change in volume, $\Delta E_p = (4\pi/3)(r_{\rm vir}^3 - r_f^3)P_s$. The equation for conservation of energy is thus

$$E_f = \sum_{r_k<r_f} \left[\rho_0 \theta_k^{1/(\Gamma-1)} \phi_k + \tfrac{3}{2}(1+2\delta_{\rm rel}) P_0 \theta_k^{\Gamma/(\Gamma-1)}\right] l^3 = E_g + \Delta E_P + \epsilon_f M_\star c^2. \quad (7)$$

The term $\epsilon_f M_\star c^2$ is feedback inferred from supernovae and AGNs, discussed in more detail below. Matching the final surface pressure to the external pressure yields the other equation of constraint,

$$(1+\delta_{\rm rel}) N_{b,f}^{-1} \sum_{k=1}^{N_{b,f}} P_0 \theta_k^{\Gamma/(\Gamma-1)} = P_s, \quad (8)$$

again summing in a buffer region $r_f < r < r_f + 9l$. (Note that the $\delta_{\rm rel}$ terms were omitted in Ostriker et al. [2005].) With equations (7) and (8) it is possible to iterate (e.g., with Newton-Raphson) to a solution for the final gas density and pressure (or temperature) profile.

For this paper we will assume that at $z = 0$ the initial (that is, inside $r_{\rm vir}$ prior to any rearrangement) star-to-gas ratio is 10%; in other words, $f_\star = M_\star/M_g = 0.10$, which implies $M_\star = (f_c M_{\rm vir}) f_\star/(1+f_\star)$. This ratio agrees well with the value in nearby clusters measured by Lin et al. (2003) and is slightly lower than that measured by Voevodkin & Vikhlinin (2004). Star and black hole formation will return energy to the remaining gas via supernova and AGN activity; writing this energy as $\epsilon_f M_\star c^2$ of course assumes this energy is proportional to stellar mass. This seems plausible; the number of supernovae is expected to be proportional to the mass in stars, and the mass of central black holes in spheroids is roughly proportional to the stellar mass in these systems (Merritt & Ferrarese 2001; Kormendy & Gebhardt 2001). Improved observational constraints may alter this assumption. The rough estimate given in Ostriker et al. (2005) is that $\epsilon_f \approx 3\times10^{-6}$ for supernovae and $\epsilon_f \approx 4\times10^{-5}$ for AGNs, so we will take $\epsilon_f = 5\times10^{-5}$ as the maximum case. This is roughly 3 keV particle^{-1} for the gas inside the virial radius, which is at the high end of the plausible range.

2.3. *Cluster Temperature*

To characterize the temperature of the gas we will use $T_{\rm ew}$, the X-ray-emission–weighted T inside a projected radius of R_{500}. The X-ray luminosity is calculated using the cooling function $\Lambda(T)$ of Maller & Bullock (2004) for $T \le 10^8$ K, and assuming $\Lambda(T) \propto T^{0.5}$ for $T > 10^8$ K; the metallicity is set to one-third solar (Baumgartner et al. 2005). Mazzotta et al. (2004) showed that the projected spectroscopic temperature of a thermally complex cluster will in fact be lower than the emission-weighed temperature. However, this difference will be more pronounced when computing a single-temperature fit to a full hydrodynamic simulation (containing shocks, cold fronts, and other short-lived structures) than it is in our simple equilibrium models (which lack such local inhomogeneities), because such features, which increase the thermal complexity of the gas, contribute to this systematic bias (Mazzotta et al. 2004; Kawahara et al. 2007). In order to quantify this effect, we compared $T_{\rm ew}$ with $T_{\rm sp}$, the spectroscopic temperature measured in the range $0.15R_{500} \le R \le R_{500}$. We used the code[4] developed by Vikhlinin (2006) to compute $T_{\rm sp}$, using the *Chandra* response function and Galactic absorption $N_{\rm H} = 2\times10^{20}$ cm^{-2}. Note that simply excluding the center reduces the measured $T_{\rm sp}$ relative to $T_{\rm ew}$, independent of spectral effects. For the maximum-feedback model, we find $kT_{\rm sp} = 0.94kT_{\rm ew} - 0.06$ keV with little scatter; in other words, the two agree within 10%. Given this small difference, we will use the conceptually simpler $T_{\rm ew}$, unless stated otherwise.

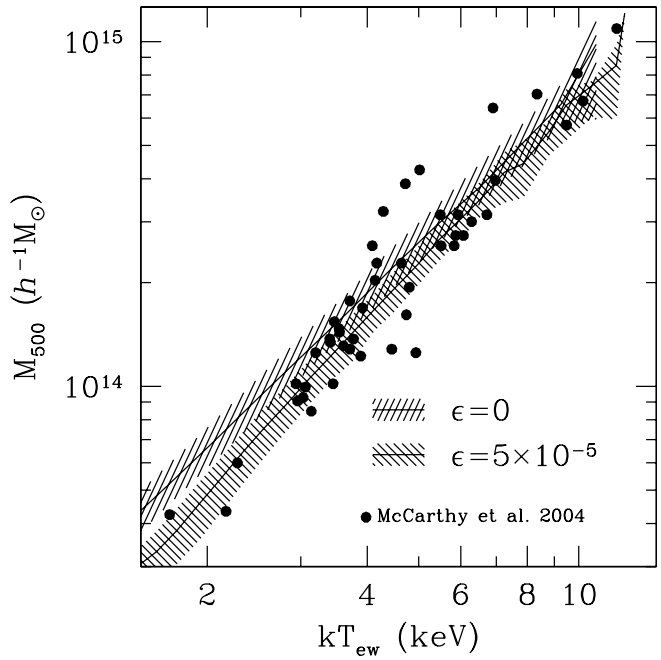

FIG. 1.—M-$T_{\rm ew}$ relation for two values of the feedback parameter; $T_{\rm ew}$ is the emission-weighted temperature from all material inside projected r_{500}. Lines show the median value, and shaded regions enclose 68% of the clusters. Filled circles are data described in McCarthy et al. (2004) using only $z < 0.06$ clusters. [*See the electronic edition of the Journal for a color version of this figure.*]

3. EFFECTS OF FEEDBACK

3.1. *Gas Temperature*

X-ray surveys provide valuable information on the luminosity, temperature, and mass of clusters. In this section we explore these properties as derived using the method of § 2.3 The relationship between mass and temperature is shown in Figure 1. The temperature is the emission-weighted $T_{\rm ew}$ inside a projected radius R_{500}, and the mass is that contained in a spherical overdensity of 500 times critical, r_{500}. Lines show the median mass at a given temperature, and the shaded regions enclose 68% of the clusters; the cases with no feedback ($\epsilon_f = 0$) and maximum feedback ($\epsilon_f = 5\times10^{-5}$) are shown. Feedback has little effect for the hottest, most massive clusters; the feedback energy is small compared to the binding energy of these clusters and thus is of little importance to the dynamical state of the gas. Feedback has a greater effect in less massive clusters, making the gas somewhat hotter. Still, at $M_{500} \approx 5\times10^{13}\ h^{-1}\ M_\odot$, feedback

[4] Available at http://hea-www.harvard.edu/∼alexey/mixT.

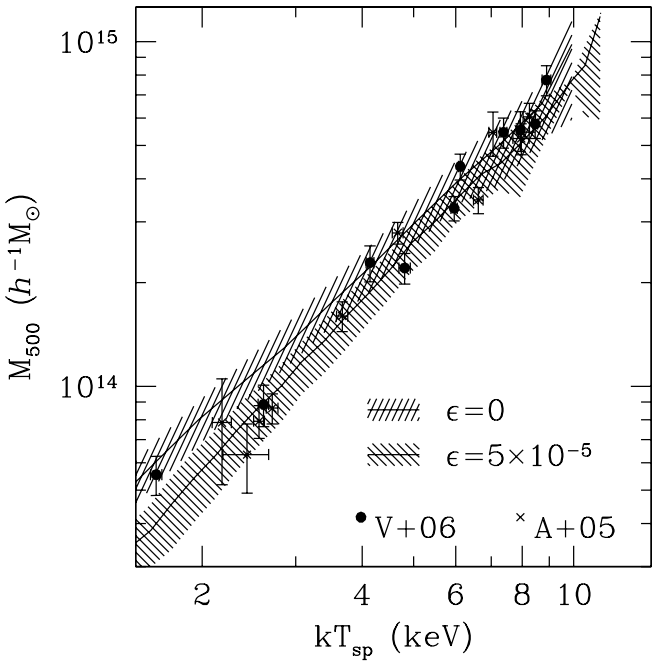

FIG. 2.—M-T_{sp} relation for two values of the feedback parameter; T_{sp} is the spectroscopic temperature excluding the inner $0.15r_{500}$. Lines show the median value, and shaded regions enclose 68% of the clusters. Filled circles are from Vikhlinin et al. (2006), and crosses are from Arnaud et al. (2005). [*See the electronic edition of the Journal for a color version of this figure.*]

increases T by only ~33%. One effect not apparent from the figure is that for masses below $M_{500} \approx 3 \times 10^{13}\ h^{-1}\ M_\odot$, the maximum feedback can be enough to make the total gas energy positive, unbinding the gas from the halo. Thus, our method produces no halos with temperatures below about 1.5 keV in the maximum-feedback case. The data points shown in this figure are from McCarthy et al. (2004), who combined *ASCA* observations with the extended *Röntgensatellit* (*ROSAT*) HIFLUGCS sample of Reiprich & Böhringer (2002); cluster cores were not excluded when $T$was determined. Only those clusters closer than $z < 0.06$ are shown. Below 4 keV, the feedback model provides a superior fit; both models are in agreement with the data above this. However, there is significantly more scatter in the observed M-T relation than is produced in our model. Cooling (which we neglect beyond that involved in star formation) will increase the scatter in this relation (McCarthy et al. 2004; O'Hara et al. 2006). The existence of young systems which are out of dynamical equilibrium can also broaden the observed M-T relation, but the effects may not be very pronounced (O'Hara et al. 2006); we are to some extent accounting for this, because merging halos will have greater KE per particle and thus a higher temperature than a relaxed halo of the same mass. We have not modeled observational error, which will also, of course, add to any intrinsic scatter.

As shown in Figure 2, our predicted M-T relations change little if we instead use the spectroscopic temperature. Also shown are 10 nearby relaxed clusters observed with *XMM-Newton* by Arnaud et al. (2005) and 10 relaxed clusters observed with *Chandra* by Vikhlinin et al. (2006). Both used spectroscopic temperatures and excluded the cores (although the radial range used to determine T is slightly different). These observations exhibit considerably smaller scatter, lending credence to the idea that differing dynamical states and cooling in cores will increase the scatter in temperature at a given mass. As was the case before, both models agree reasonably well with the observed M-T relation above 4 keV, but the high-feedback case is a better fit in the 2–3 keV range. The M-T relation can be well fit by the power law

$$E(z)\frac{M_{500}}{10^{14}\ h^{-1}\ M_\odot} = A\left(\frac{kT}{5\ \mathrm{keV}}\right)^{\alpha}, \qquad (9)$$

where $E(z) = H(z)/H_0$. Arnaud et al. (2005) found $A = 2.69 \pm 0.10$ and $\alpha = 1.71 \pm 0.09$ for their sample, while Vikhlinin et al. (2006) obtained $A = 2.89 \pm 0.15$, $\alpha = 1.58 \pm 0.11$. We first attempted to fit this relation to the simulated halos with ordinary least-squares regression in the log-log plane, but this was dominated by the more numerous low-mass halos and unduly affected by outliers. Thus, we instead adopted the following procedure. We divided the x-axis into 20 logarithmically spaced bins, calculated the median in each bin, and then found the best fit to these points. This in effect gives more massive clusters a higher weight in the fitting; the resulting fits follow closely the median lines in the figures. As listed in Table 2, fitting to all halos with $kT_{sp} \geq 3$ keV in the zero-feedback model gives $A = 3.12$ and $\alpha = 1.49 \pm 0.02$. This follows the self-similar slope of 1.5, and gives cooler clusters at a fixed mass than is observed. In the maximum-feedback case, temperatures shift to higher values, and the slope becomes steeper: $A = 2.56$ and $\alpha = 1.62 \pm 0.03$. This slope agrees well with the observations, although the normalization yields slightly hotter clusters at a given mass. The formal error we obtain for A is small (near 1%), so in Table 2 we give the rms fractional difference (in percent) of the halos from the best-fit relation; this scatter reflects well the width of the shaded regions in the figures. If the amount of feedback ϵ_f varied from cluster to cluster, then the scatter seen would be larger.

Another method of characterizing nearby clusters is the temperature function, which does not require a mass determination. The distribution of cluster temperatures is sensitively dependent on the cosmological model; in Ostriker et al. (2005), which used the *WMAP* first year power spectrum amplitude, the fit to observations was inadequate. Shown in Figure 3 are two measurements of the cumulative temperature function with different methods of determining the cluster temperature; Ikebe et al. (2002) excluded cluster cores when fitting for T, while Henry (2004) did not. For purposes of comparison, we took from the simulation a "light cone" covering one octant of the sky out to $z = 0.2$. This covers the redshift range used in the observations,

TABLE 2
POWER-LAW FIT PARAMETERS

Relation	$\epsilon_f = 0$		$\epsilon_f = 5 \times 10^{-5}$	
	A	α	A	α
kT_{sp}-M_{500}	0.46 ± 9	0.67 ± 0.01	0.55 ± 10	0.60 ± 0.01
M_g-M_{500}	1.44 ± 10	0.96 ± 0.01	0.80 ± 12	1.17 ± 0.02
L_X-M_{500}	1.15 ± 26	1.13 ± 0.02	0.31 ± 25	1.59 ± 0.03
L_{SZ}-M_{500}	0.43 ± 25	1.62 ± 0.02	0.35 ± 31	1.69 ± 0.03
M_{500}-kT_{sp}	3.12 ± 14	1.49 ± 0.02	2.56 ± 19	1.62 ± 0.03
M_g-kT_{sp}	4.37 ± 17	1.40 ± 0.03	2.42 ± 24	1.84 ± 0.06
L_X-kT_{sp}	4.09 ± 29	1.66 ± 0.03	1.36 ± 34	2.51 ± 0.08
L_{SZ}-kT_{sp}	2.86 ± 15	2.43 ± 0.03	1.85 ± 16	2.77 ± 0.04

NOTES.—For each relation Y-X, the best-fit parameters of the form $Y/Y_0 = A(X/X_0)^\alpha$ are given. For $Y = (M_{500}, kT_{sp}, M_g, L_X, L_{SZ})$, $Y_0 = (10^{14}\ h^{-1}\ M_\odot$, 5 keV, $10^{13}\ h^{-1}\ M_\odot$, $10^{44}\ h^{-2}$ ergs s^{-1}, $10^{14}\ h^{-1}$ keV $M_\odot)$. When $X = M_{500}$, the fit is to all halos with $X \geq X_0 = 10^{14}\ h^{-1}\ M_\odot$; when $X = kT_{sp}$, $X_0 = 5$ keV, and the fit is to all halos with $kT_{sp} \geq 3$ keV. The scatter given for A is the rms fractional difference (in percent) of the halos from the best-fit relation.

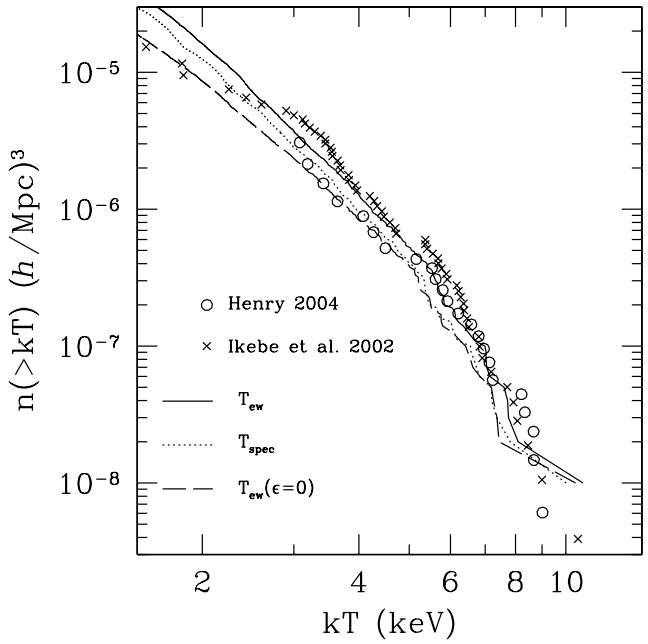

FIG. 3.—X-ray temperature function. Crosses are from Ikebe et al. (2002), who excluded cluster cores, and circles are from Henry (2000), who kept them. Lines are the volume-limited $z < 0.2$ temperature function from simulated clusters (*solid*: emission-weighted $T_{\rm ew}$ from all material inside projected R_{500}; *dotted*: spectroscopic $T_{\rm spec}$ excluding the inner $0.15R_{500}$; *dashed*: emission-weighted $T_{\rm ew}$ with no feedback). [*See the electronic edition of the Journal for a color version of this figure*.]

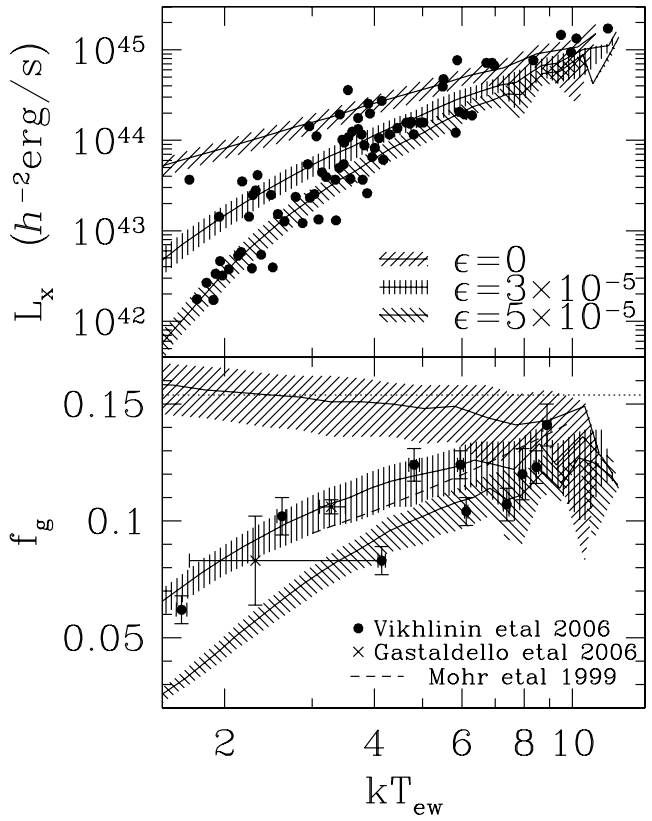

FIG. 4.—*Top*: $L_{\rm X}$-T relation for three values of the feedback parameter. For the simulated $z = 0$ clusters, the lines are the median and the shaded regions enclose 68% of the clusters. Filled circles are data described in McCarthy et al. (2004) using only $z < 0.06$ clusters. *Bottom*: Gas fraction inside r_{500}. Points with error bars are data from Vikhlinin et al. (2006) and Gastaldello et al. (2006) and the dashed line is the best fit to 45 *ROSAT* clusters by Mohr et al. (1999). The dotted line is the cosmic mean adjusted to make the global star/gas ratio 10%. [*See the electronic edition of the Journal for a color version of this figure*.]

although they are not volume limited. During the simulation, the matter distribution in a series of thin shells was saved; the radius of each shell corresponds to the light travel time from a $z = 0$ observer sitting at the origin of the box, and its width corresponds to the time interval between shells. Thus, a volume-limited mass distribution, including time evolution, is obtained. Locating halos and adding gas was done in the same manner as before. To compute the star/gas ratio at $z > 0$, the star formation rate was assumed to follow a delayed exponential model (eq. [1] of Nagamine et al. 2006) with decay time $\tau = 1$ Gyr. Both $T_{\rm ew}$ and $T_{\rm sp}$ are shown for the $\epsilon_f = 5 \times 10^{-5}$-feedback model in Figure 3. Because our cosmological parameters were chosen in part to match large-scale structure observations, and the simulated M_{500}-T relation matches that of nearby clusters, it is not surprising that our simulated temperature function is a reasonable fit to that observed. Our $T_{\rm ew}$, which includes the core, gives a higher abundance in the 3–6 keV range than the Henry (2004) data, while our $T_{\rm sp}$, excluding the core, instead gives a lower abundance than Ikebe et al. (2002). The zero-feedback model appears to give temperatures that are too low; thus, based simply on T, it appears that some nongravitational energy input is required to explain the properties of existing clusters. The model with feedback and *WMAP* 3 year cosmological parameters now provides a good fit to the observed temperature function.

3.2. *Gas Density*

Other cluster observables are more dependent on the gas density, most notably X-ray luminosity. The top panel of Figure 4 shows the $L_{\rm X}$-T relation of our simulated catalog for three values of feedback, again with medians shown as lines and shaded regions enclosing 68% of the clusters; here $L_{\rm X}$ is the bolometric luminosity inside a projected radius of R_{500}. Unlike the M-T relation, feedback produces a significant change in $L_{\rm X}$ at a given temperature, because the bremsstrahlung emission is proportional to the square of the gas density, but otherwise, there are similar trends seen. Again, the effect of feedback is less important in the most massive clusters, where gravitational binding energy dominates. The scatter for a given amount of feedback is also much smaller than that observed in nearby clusters (the data points are again from McCarthy et al. [2004] with $z < 0.06$). The zero feedback and $\epsilon_f = 5 \times 10^{-5}$ models bracket the range of luminosities seen in nearby clusters. An intermediate model with $\epsilon_f = 3 \times 10^{-5}$ is also shown in Figure 4; it appears this is an insufficient amount to explain the lowest luminosity clusters. Fitting a power law $L_{\rm X}/(10^{44}\ h^{-2}\ {\rm ergs\ s^{-1}}) = A(kT_{\rm sp}/5\ {\rm keV})^{\alpha}$ to all our halos with $kT_{\rm sp} \geq 3$ keV yields $\alpha = 1.66 \pm 0.03$ in the zero-feedback case, not as steep as the self-similar expectations of $L_{\rm X} \propto T^2$. Including feedback steepens this relation considerably to $\alpha = 2.51 \pm 0.08$, more in line with the observed value (e.g., Arnaud & Evrard 1999; Reiprich & Böhringer 2002; Ikebe et al. 2002). The exact value of the slope we find depends on the lower temperature limit used.

A more direct probe of gas density is the gas fraction within a given radius. It appears that the gas fraction increases with increasing radius, and higher temperature clusters have a higher gas fraction as well (David et al. 1995; Arnaud & Evrard 1999; Mohr et al. 1999; Vikhlinin et al. 2006). The gas fraction from our model is shown in the bottom panel of Figure 4, with f_g defined as the fraction of the total mass inside a spherical radius r_{500} enclosing an overdensity 500 times critical; for the purpose of computing the total mass, we assumed that stellar mass

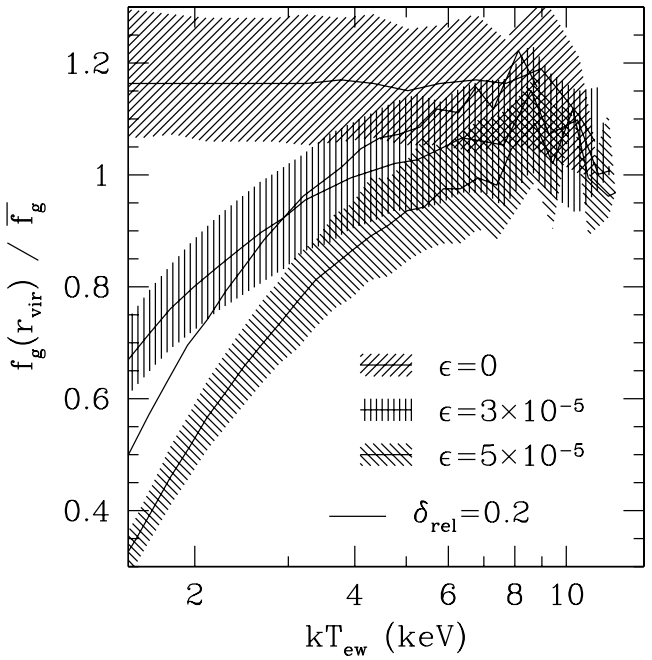

FIG. 5.—Gas fraction inside the virial radius r_{vir}, normalized to the cosmic mean value (adjusted for star formation), as a function of temperature. Lines are the median and shaded regions enclose 68% of the clusters. The line without shading is the median for $\epsilon_f = 5\times10^{-5}$ and $\delta_{rel} = 0.20$. [*See the electronic edition of the Journal for a color version of this figure.*]

followed the same radial profile as the dark matter. The model curves display the type of behavior one might expect based on the top panel; models with feedback show significantly lower gas fractions (i.e., lower densities at a given T) with the effect being most pronounced for the lowest mass clusters. Recent observations of the gas fraction by Vikhlinin et al. (2006) are shown in the figure, as well as two clusters from Gastaldello et al. (2006), where the temperature was derived from M_{500} using the M-T relation of Vikhlinin et al. (2006) for these points; note that they use a spectroscopic temperature and exclude the central region when finding T. Also shown as a dashed line is the best-fit f_g-T relation found by Mohr et al. (1999) using 45 *ROSAT* clusters and temperatures taken from the literature. Here again, some feedback is required to bring the models in agreement with observed gas fractions, but again, the spread in any given model is too small to fit all observed values of f_g.

Also shown as a dotted line in the figure is the mean gas fraction from our cosmological model, after turning enough gas into stars to make the global star/gas ratio 10%, or $\overline{f_g} = f_c[1 - f_\star/(1 + f_\star)]$. Without any feedback, the baryon fraction inside r_{500} will reflect the cosmic mean value, but energy input drives this fraction lower, particularly for smaller clusters. We find the gas fraction increases with radius, so at overdensities higher than 500, this discrepancy will be even greater. This raises the question of how far out one must go before the cluster contains a fair sample of the cosmic mass budget. Figure 5 shows the median gas fraction inside the virial radius as a function of temperature (still using T_{ew} inside r_{500}); the virial overdensity is 97 times critical for our chosen cosmology. Even at this radius, it is only for the most massive clusters ($kT_{ew} \gtrsim 6$ keV) that the baryon fraction reaches the cosmic mean; in smaller clusters feedback causes the gas to expand, reducing the gas fraction by many tens of percent. Attempts to determine the cosmic baryon density from clusters will need to take this effect into account.

Figure 5 also demonstrates how the median gas fraction changes in the maximum-feedback case if we also add a relativistic component with $\delta_{rel} = 0.20$ (there is little change in the spread around the median). With this component, a lower temperature is required to achieve pressure balance at a given density. This model behaves like the no-feedback case at higher masses and like an intermediate-feedback case at lower masses. This behavior also holds for all the other relationships (M_{500}-T_{ew}, L_X-T_{ew}, etc.) explored in this paper; thus, it seems a relativistic component will have little effect on thermal cluster observables. While our implementation is quite simplified, similar results were found using full hydrodynamic simulations by Pfrommer et al. (2007); they found that including the effects of cosmic rays caused only small changes in the gas fraction and integrated SZ signal (they found a larger change in L_X, but this was related to cooling cores, which we do not implement).

To summarize this section, we find that a *WMAP* 3 year cosmological model coupled with a feedback parameter of $\epsilon_f = (3\text{–}5)\times10^{-5}$ (which corresponds to an input energy of roughly 2–3 keV baryon^{-1}) provides a good fit to the extant X-ray observations of hot gas in clusters.

4. DISCUSSION

In this paper we have presented a method for determining the gas distribution inside a fully three-dimensional potential; this method assumes hydrostatic equilibrium and a polytropic equation of state, and also that the original gas energy per unit mass equals that of the DM. We then applied this method to a $z = 0$ catalog of DM cluster halos drawn from N-body simulations, and compared the resulting ICM distributions to observations of nearby clusters. The main result is that this simple gas prescription can reproduce many of the observed bulk properties of the ICM, including the temperature distribution and the relationships between temperature and mass, X-ray luminosity, or gas fraction. The main drawback is that in nearby X-ray clusters there is significantly more scatter seen in these relationships than is produced in our method. This could be due to a number of factors, including cooling cores, our assumption of hydrostatic equilibrium, and observational errors.

The advantages of using this type of model for the ICM are clear. It is possible to simulate a large volume with a N-body code at much smaller computational cost than is required for a full hydrodynamical treatment. When adding gas with the method described here, the distributions of internal halo properties (concentration, triaxiality, substructure, etc.) are taken into account, as are their trends with mass, location, and time, plus any alignments and correlations between halos. However, it should be noted that this approach does not account for the dynamical effects of a baryonic component. Results from halo formation simulations demonstrate that including a dissipational gas component can alter the radial profile of the DM halo (Gnedin et al. 2004; Lin et al. 2006) and its ellipticity (Kazantzidis et al. 2004), which would in turn alter the ICM distribution.

A second result is that a significant amount of nongravitational energy input is required to reproduce the properties of nearby clusters. Many other investigators have reached the same conclusion (e.g., Kaiser 1991; Balogh et al. 1999; Suto et al. 1998; Wu et al. 2000; Loewenstein 2000; Tozzi & Norman 2001; Komatsu & Seljak 2001; Babul et al. 2002; Voit et al. 2002; Dos Santos & Doré 2002; Shimizu et al. 2004; Lapi et al. 2005; Afshordi et al. 2005; Solanes et al. 2005). In this paper we do not try to find the sources of this input. Instead, we simply ascertain what level of feedback would produce the observed relations among cluster observables. Processes involved in star formation provide some of this energy, but not enough. The most likely source for extra energy is AGNs, which can conceivably deliver enough feedback

to explain the temperature, X-ray luminosity, and gas fraction distributions of local clusters. However, there is little margin for error; if we have overestimated the amount of star formation, the black hole–to–stellar mass ratio is less than 0.0013, and/or the amount of energy returned to the gas by black hole formation is less than 3% of the black hole rest mass, then the required energy of 2–3 keV particle^{-1} will not be produced. This conclusion differs somewhat from that of McCarthy et al. (2007), who find that AGN heating is an implausible (although not impossible) explanation of cluster gas fractions; they calculate that in order to reduce the gas fraction within r_{500} to the observed level, it would take 10 keV particle^{-1} in the gas observed within r_{500} (roughly $0.12M_{500}$). Rescaling this value to our normalization (energy per particle of the gas mass initially inside $r_{\rm vir}$, or $f_c M_{\rm vir}$), makes this a required energy of roughly 4 keV particle^{-1}. The reason we require less energy is in part due to a different initial state; examining the bottom panel of Figure 4, by just accounting for star formation but not including any feedback, one can see our method leads to a gas fraction inside r_{500} already lower than the cosmic mean, while McCarthy et al. (2007) started with a state in which the gas fraction equals the cosmic mean. (Although in any case they argue that efficiencies of AGN outbursts are $\sim 10^{-3}$, not $\sim 10^{-1}$.) By running hydrodynamic simulations without radiation or feedback, Crain et al. (2006) found the baryon fraction inside r_{500} of 90%, which agrees well with our method at higher masses. However, Crain et al. (2006) also find this fraction still holds at lower masses and that the baryon fraction is still 90% at the virial radius (again with no feedback), while we find a higher fraction in both of these instances. Note that if we had instead started with an initial state consistent with a 90% baryon fraction, then we would require a lower amount of feedback to reproduce observed gas fractions.

It is useful in this context to compare with recent hydrodynamical simulations which include feedback. The left panel of Figure 6 relates gas to total mass inside r_{500}; the solid line shows the best-fit power-law relation at $z = 0$ found from adaptive refinement simulations by Kravtsov et al. (2006). With no feedback we find a similar slope (slightly larger than unity), but for a given halo mass there is a higher gas fraction than in the simulations. Adding feedback reduces this discrepancy at higher masses, but at lower masses our maximum-feedback case instead has lower gas fractions. As Kravtsov et al. (2006) did not attempt to include AGN feedback, it is not surprising that an intermediate amount of feedback would provide the best match. We do not match the simulations when it comes to the total mass-temperature relation, however. For equation (9), Kravtsov et al. (2006) find $A = 3.85 \pm 0.19$ and $\alpha = 1.524 \pm 0.07$, while Kay et al. (2007), with a smoothed particle hydrodynamics (SPH) simulation, find $A = 4.47 \pm 0.19$ and $\alpha = 1.76 \pm 0.07$. We obtain a similar slope ($\alpha = 1.62$), but more importantly we find a different normalization; that is, we find hotter temperatures at a given mass, as would be expected, because we included a higher level of feedback.

The near future will see a number of surveys that select clusters of galaxies via their Sunyaev-Zel'dovich (SZ) decrement, which is proportional to the gas pressure in the cluster integrated along the line of sight. Currently, the Sunyaev-Zel'dovich Array (SZA; Carlstrom et al. 2000) and the Arcminute Microkelvin Imager (AMI; Kneissl et al. 2001) are equipped to perform such a search on tens of square degrees on the sky. However, the Atacama Cosmology Telescope (ACT), the South Pole Telescope (SPT), the Atacama Pathfinder Experiment (APEX), and ultimately, the *Planck Surveyor* will scan thousands of square degrees on the sky in the radio (Ruhl et al. 2004; Fowler 2004;

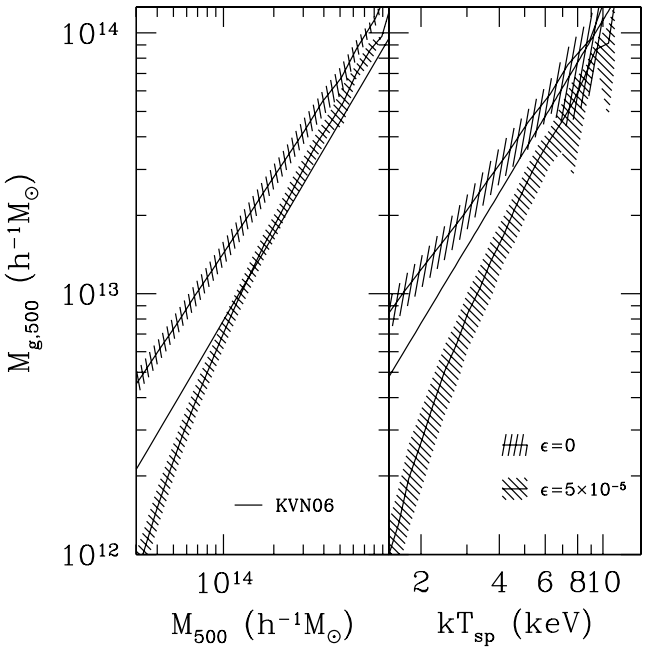

FIG. 6.—Gas mass inside r_{500} as a function of M_{500} (*left*) and $kT_{\rm sp}$ (*right*). The straight lines are the full hydrodynamic simulation result from Kravtsov et al. (2006). Lines are the median and shaded regions enclose 68% of the clusters. [*See the electronic edition of the Journal for a color version of this figure.*]

Güsten et al. 2006; Clavel & Tauber 2005). These surveys will detect thousands of clusters; for example, the SPT will scan 4000 deg^2 on the sky and observe on the order of 6000 clusters of galaxies (this is for a flux sensitivity of about 1.5 mJy at the 4 σ detection threshold with a $1'$ beam operating at 150 GHz and assumes $\sigma_8 = 0.75$). This translates to a limiting mass of $M_{\rm lim} \approx 10^{14.2}\ h^{-1}\ M_\odot$ if one assumes the clusters are in hydrostatic equilibrium. Sehgal et al. (2007) found a similar limit for a 90% complete cluster sample from ACT.

The redshift distribution of clusters is very sensitive to the amplitude and growth of linear perturbations and, hence, to cosmological parameters (Holder et al. 2001; Haiman et al. 2001; Weller et al. 2002; Battye & Weller 2003; Majumdar & Mohr 2004; Younger et al. 2006). However, in order to exploit SZ cluster number counts, one is required to understand the selection function of these surveys. This is most easily accomplished in terms of the flux decrement, which depends on the system temperature, exposure time, bandwidth, and efficiency (Battye & Weller 2005). In order to obtain cosmological constraints, it is necessary to convert the observables into a limiting mass of the survey. There are two approaches to obtain this mass limit. One is to start with the assumption that all clusters are spherical and in hydrostatic equilibrium, and then include some nuisance parameters to allow for deviations from this assumption (Verde et al. 2002; Battye & Weller 2003; Younger et al. 2006). Another approach is to use a very general parameterization of the mass-observable relation, which in its most general form could easily introduce 40 unknown parameters (Hu 2003; Lima & Hu 2005). Currently, there is little data to constrain the free parameters in either approach. In the future one can exploit the SZ cluster observations themselves to self-calibrate these free parameters (Hu 2003; Lima & Hu 2005; Majumdar & Mohr 2004; Battye & Weller 2003). However, if one employs the most general parameterization, little power is left in the surveys to constrain cosmological parameters (Hu 2003; Lima & Hu 2005). Another possibility would be to use complementary observations, such as weak lensing to cross-calibrate the mass-observable

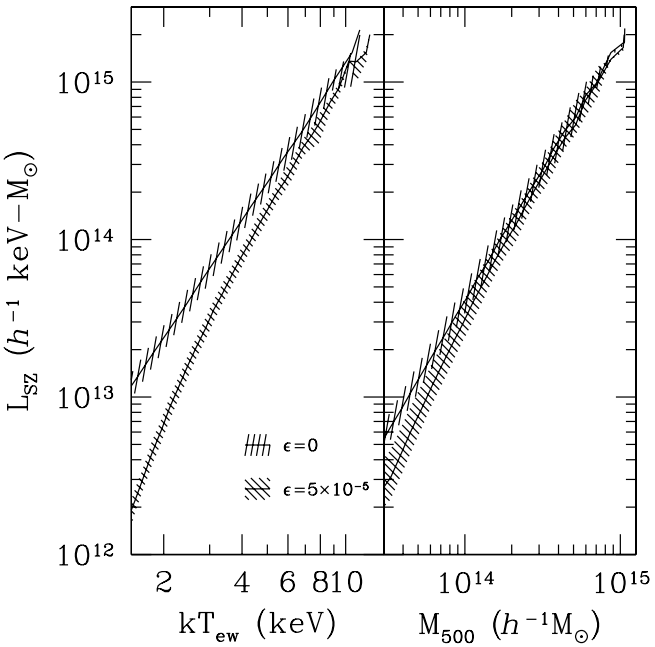

FIG. 7.—Integrated SZ decrement, $L_{SZ} = \int dA \int \rho kT\, dl$, as a function of temperature (*left*) and mass (*right*), for two values of the feedback parameter. Lines show the median value, and shaded regions enclose 68% of the clusters. [*See the electronic edition of the Journal for a color version of this figure.*]

relation (Majumdar & Mohr 2004; Abbott et al. 2005; Sealfon et al. 2006). A useful approach would be to have a physical parameterization of the mass-observable relation with some prior probability on the free parameters and then self-calibrate the SZ surveys for these parameters (Younger et al. 2006). However, in order to obtain this prior knowledge, we cannot yet rely on observations, because currently they are sparse, and in the near future, observations will not resolve clusters, because the beams of the instruments are typically larger than $1'$. We therefore require simulations to explore the scatter in the mass-observable relation; in order to obtain realistic results, a large representative sample of galaxy clusters is required.

Sehgal et al. (2007) have already applied the method of this paper to a full light-cone N-body output (out to $z = 3$) in order to generate and make publicly available large-area, subarcminute-resolution microwave sky maps. We intend to provide a detailed analysis of the mass-observable relation in a forthcoming paper and will give here only a rough qualitative discussion. In particular, we can use our $z = 0$ simulated catalog to explore how the amount of thermal energy in the gas will affect the SZ signal. One can express the strength of the integrated SZ flux as

$$L_{SZ} = \int dA \int \rho kT\, dl, \tag{10}$$

where the integration limits are along the line of sight through the entire cluster and over area out to projected radius r_{500}. The right panel of Figure 7 displays how the SZ signal varies with cluster mass in our model for the zero- and maximum-feedback cases. At higher masses the relation has little dependence on feedback. Feedback reduces the SZ signal somewhat (as it results in gas being pushed out of the higher pressure cluster cores) and makes the relation steeper. Fitting to halos with $M_{500} \geq 10^{14}\ h^{-1}\ M_\odot$, we find $L_{SZ} \propto M_{500}^{1.62}$ with zero feedback. This is close to the self-similar slope of 5/3 predicted for spherical profiles (e.g., Reid & Spergel 2006); apparently, triaxiality and substructure have little effect on this relation. The slope steepens only slightly to 1.69 for $\epsilon_f = 5 \times 10^{-5}$; this is in reasonable agreement with the analytic results of Reid & Spergel (2006) and with hydrodynamic simulations (White et al. 2002; da Silva et al. 2004; Motl et al. 2005; Nagai 2006). The exact slope found for this relation depends on the lower mass limit used; if we included lower mass halos (or weighted the high-mass halos less), the resulting slope would be steeper. The left panel of Figure 7 shows how L_{SZ} varies with temperature. The relation is quite tight and again steepens with increasing feedback; in fitting to halos with $kT_{sp} \geq 3$ keV, $L_{SZ} \propto T_{sp}^{2.43}$ with no feedback, and the exponent increases to 2.77 for $\epsilon_f = 5 \times 10^{-5}$. The zero-feedback slope agrees well with the adiabatic simulation of Nagai (2006), but the feedback model is steeper, because we are putting in more energy. Increasing ϵ_f from zero to $\epsilon_f = 5 \times 10^{-5}$ lowers the SZ signal at $kT_{ew} = 5$ keV by 35%, which is similar to, but slightly less than, the effect seen by Nagai (2006) between his adiabatic and star formation runs. A more detailed comparison is difficult, because we are using the projected SZ signal; there are also differences in the cosmological parameters.

This work makes it clear that allowance for feedback will be necessary if one is to use the upcoming SZ surveys for precision measurements of cosmological parameters. Fortunately, X-ray observations allow us to calibrate the feedback parameter; adequate fits to the data can be obtained if the ratio of energy input to stellar mass is $\epsilon_f = (3\text{–}5) \times 10^{-5}$. Uncertainties in this parameter will propagate into uncertainties in the mass-flux decrement relation for SZ surveys. However, it can be seen in Figure 7 that even the extreme case of reducing ϵ_f to zero hardly changes this relation for clusters with masses above $2 \times 10^{14}\ h^{-1}\ M_\odot$. Moreover, it is not the scatter in the mass-observable relation which makes it difficult for future SZ surveys to constrain cosmological parameters, but rather it is the uncertainty in the scatter which is the main problem (Lima & Hu 2005). We will use the methods of this paper to explore these issues in future work.

The authors would like to thank Niayesh Afshordi for useful email exchanges and Ian McCarthy for making available the observational data. We also thank the anonymous referee for a careful and helpful reading of the manuscript. This work was partially supported by the National Center for Supercomputing Applications under grant MCA04N002; in addition, computational facilities at Princeton supported by NSF grant AST 02-16105 were used, as well as high performance computational facilities supported by Princeton University under the auspices of the Princeton Institute for Computational Science and Engineering (PICSciE) and the Office of Information Technology (OIT).

REFERENCES

Abbott, T., et al. 2005, The Dark Energy Survey (Batavia: Fermilab) (astro-ph/0510346)
Afshordi, N., Lin, Y.-T., & Sanderson, A. J. R. 2005, ApJ, 629, 1
Allgood, B., Flores, R. A., Primack, J. R., Kravtsov, A. V., Wechsler, R. H., Faltenbacher, A., & Bullock, J. S. 2006, MNRAS, 367, 1781
Arnaud, M., & Evrard, A. E. 1999, MNRAS, 305, 631
Arnaud, M., Pointecouteau, E., & Pratt, G. W. 2005, A&A, 441, 893
Ascasibar, Y., Sevilla, R., Yepes, G., Müller, V., & Gottlöber, S. 2006, MNRAS, 371, 193
Ascasibar, Y., Yepes, G., Müller, V., & Gottlöber, S. 2003, MNRAS, 346, 731
Avila-Reese, V., Firmani, C., Klypin, A., & Kravtsov, A. V. 1999, MNRAS, 310, 527

Babul, A., Balogh, M. L., Lewis, G. F., & Poole, G. B. 2002, MNRAS, 330, 329
Balogh, M. L., Babul, A., & Patton, D. R. 1999, MNRAS, 307, 463
Bartelmann, M., Dolag, K., Perrotta, F., Baccigalupi, C., Moscardini, L., Meneghetti, M., & Tormen, G. 2005, NewA Rev., 49, 199
Battye, R. A., & Weller, J. 2003, Phys. Rev. D, 68, 083506
———. 2005, MNRAS, 362, 171
Baumgartner, W. H., Loewenstein, M., Horner, D. J., & Mushotzky, R. F. 2005, ApJ, 620, 680
Berlind, A. A., Kazin, E., Blanton, M. R., Pueblas, S., Scoccimarro, R., & Hogg, D. W. 2006, ApJ, submitted (astro-ph/0610524)
Bertschinger, E. 2001, ApJS, 137, 1
Bode, P., & Ostriker, J. P. 2003, ApJS, 145, 1
Bode, P., Ostriker, J. P., & Xu, G. 2000, ApJS, 128, 561
Borgani, S., Finoguenov, A., Kay, S. T., Ponman, T. J., Springel, V., Tozzi, P., & Voit, G. M. 2005, MNRAS, 361, 233
Borgani, S., et al. 2006, MNRAS, 367, 1641
Bullock, J. S., Kolatt, T. S., Sigad, Y., Somerville, R. S., Kravtsov, A. V., Klypin, A. A., Primack, J. R., & Dekel, A. 2001, MNRAS, 321, 559
Carlstrom, J. E., Joy, M., Holder, G., Holzapfel, W. L., Laroque, S., Mohr, J. J., & Reese, E. 2000, in Constructing the Universe with Clusters of Galaxies, ed. F. Durret & D. Gerbal (Paris: IAP), 43
Clavel, J., & Tauber, J. A. 2005, in EAS Pub. Ser. 15, ed. L. I. Gurvits, S. Frey, & S. Rawlings (Noordwijk: ESA), 395
Comerford, J. M., Meneghetti, M., Bartelmann, M., & Schirmer, M. 2006, ApJ, 642, 39
Crain, R. A., Eke, V. R., Frenk, C. S., Jenkins, A., McCarthy, I. G., Navarro, J. F., & Pearce, F. R. 2006, MNRAS, submitted (astro-ph/0610602)
da Silva, A. C., Kay, S. T., Liddle, A. R., & Thomas, P. A. 2004, MNRAS, 348, 1401
Dahle, H., Hannestad, S., & Sommer-Larsen, J. 2003, ApJ, 588, L73
David, L. P., Jones, C., & Forman, W. 1995, ApJ, 445, 578
Diemand, J., Zemp, M., Moore, B., Stadel, J., & Carollo, C. M. 2005, MNRAS, 364, 665
Dos Santos, S., & Doré, O. 2002, A&A, 383, 450
Eke, V. R., Navarro, J. F., & Frenk, C. S. 1998, ApJ, 503, 569
Ettori, S., Dolag, K., Borgani, S., & Murante, G. 2006, MNRAS, 365, 1021
Faltenbacher, A., Kravtsov, A. V., Nagai, D., & Gottlöber, S. 2005, MNRAS, 358, 139
Fowler, J. W. 2004, Proc. SPIE, 5498, 1
Gastaldello, F., Buote, D., Humphrey, P., Zappacosta, L., Bullock, J., Brighenti, F., & Mathews, W. 2006, in The X-Ray Universe 2005, ed A. Wilson (ESA SP-604; Noordwijk: ESA), 743
Gill, S. P. D., Knebe, A., Gibson, B. K., & Dopita, M. A. 2004, MNRAS, 351, 410
Gnedin, O. Y., Kravtsov, A. V., Klypin, A. A., & Nagai, D. 2004, ApJ, 616, 16
Güsten, R., Nyman, L. Å., Schilke, P., Menten, K., Cesarsky, C., & Booth, R. 2006, A&A, 454, L13
Haiman, Z., Mohr, J. J., & Holder, G. P. 2001, ApJ, 553, 545
Henry, J. P. 2000, ApJ, 534, 565
———. 2004, ApJ, 609, 603
Hernquist, L., & Katz, N. 1989, ApJS, 70, 419
Ho, S., Bahcall, N., & Bode, P. 2006, ApJ, 647, 8
Holder, G., Haiman, Z., & Mohr, J. J. 2001, ApJ, 560, L111
Hu, W. 2003, Phys. Rev. D, 67, 081304
Ikebe, Y., Reiprich, T. H., Böhringer, H., Tanaka, Y., & Kitayama, T. 2002, A&A, 383, 773
Jing, Y. P. 2000, ApJ, 535, 30
Jing, Y. P., & Suto, Y. 2002, ApJ, 574, 538
Kaiser, N. 1986, MNRAS, 222, 323
———. 1991, ApJ, 383, 104
Kasun, S. F., & Evrard, A. E. 2005, ApJ, 629, 781
Kawahara, H., Suto, Y., Kitayama, T., Sasaki, S., Shimizu, M., Rasia, E., & Dolag, K. 2007, ApJ, 659, 257
Kay, S. T., da Silva, A. C., Aghanim, N., Blanchard, A., Liddle, A. R., Puget, J.-L., Sadat, R., & Thomas, P. A. 2007, MNRAS, in press (astro-ph/0611017)
Kazantzidis, S., Kravtsov, A. V., Zentner, A. R., Allgood, B., Nagai, D., & Moore, B. 2004, ApJ, 611, L73
Klypin, A., Kravtsov, A. V., Bullock, J. S., & Primack, J. R. 2001, ApJ, 554, 903
Kneissl, R., Jones, M. E., Saunders, R., Eke, V. R., Lasenby, A. N., Grainge, K., & Cotter, G. 2001, MNRAS, 328, 783
Komatsu, E., & Seljak, U. 2001, MNRAS, 327, 1353
Kormendy, J., & Gebhardt, K. 2001, in AIP Conf. Proc. 586, 20th Texas Symposium on Relativistic Astrophysics, ed. J. C. Wheeler & H. Martel (Melville: AIP), 363
Kravtsov, A. V., Vikhlinin, A., & Nagai, D. 2006, ApJ, 650, 128
Lapi, A., Cavaliere, A., & Menci, N. 2005, ApJ, 619, 60
Lee, J., & Suto, Y. 2003, ApJ, 585, 151
Lewis, A. D., Buote, D. A., & Stocke, J. T. 2003, ApJ, 586, 135
Lima, M., & Hu, W. 2005, Phys. Rev. D, 72, 043006
Lin, W. P., Jing, Y. P., Mao, S., Gao, L., & McCarthy, I. G. 2006, ApJ, 651, 636
Lin, Y.-T., Mohr, J. J., & Stanford, S. A. 2003, ApJ, 591, 749
Loewenstein, M. 2000, ApJ, 532, 17
Łokas, E. L., Wojtak, R., Gottlöber, S., Mamon, G. A., & Prada, F. 2006, MNRAS, 367, 1463
Lu, Y., Mo, H. J., Katz, N., & Weinberg, M. D. 2006, MNRAS, 368, 1931
Majumdar, S., & Mohr, J. J. 2004, ApJ, 613, 41
Makino, N., Sasaki, S., & Suto, Y. 1998, ApJ, 497, 555
Maller, A. H., & Bullock, J. S. 2004, MNRAS, 355, 694
Mandelbaum, R., Seljak, U., Cool, R. J., Blanton, M., Hirata, C. M., & Brinkmann, J. 2006, MNRAS, 372, 758
Mazzotta, P., Rasia, E., Moscardini, L., & Tormen, G. 2004, MNRAS, 354, 10
McCarthy, I. G., Balogh, M. L., Babul, A., Poole, G. B., & Horner, D. J. 2004, ApJ, 613, 811
McCarthy, I. G., Bower, R. G., & Balogh, M. L. 2007, MNRAS, in press (astro-ph/0609314)
Merritt, D., & Ferrarese, L. 2001, MNRAS, 320, L30
Mohr, J. J., Mathiesen, B., & Evrard, A. E. 1999, ApJ, 517, 627
Moore, B., Quinn, T., Governato, F., Stadel, J., & Lake, G. 1999, MNRAS, 310, 1147
Motl, P. M., Hallman, E. J., Burns, J. O., & Norman, M. L. 2005, ApJ, 623, L63
Muanwong, O., Kay, S. T., & Thomas, P. A. 2006, ApJ, 649, 640
Nagai, D. 2006, ApJ, 650, 538
Nagamine, K., Ostriker, J. P., Fukugita, M., & Cen, R. 2006, ApJ, 653, 881
Navarro, J. F., Frenk, C. S., & White, S. D. M. 1997, ApJ, 490, 493
Navarro, J. F., et al. 2004, MNRAS, 349, 1039
O'Hara, T. B., Mohr, J. J., Bialek, J. J., & Evrard, A. E. 2006, ApJ, 639, 64
Ostriker, J. P., Bode, P., & Babul, A. 2005, ApJ, 634, 964
Pfrommer, C., Springel, V., Jubelgas, M., & Ensslin, T. A. 2007, in Cosmic Frontiers, August 2006 (Durham), in press (astro-ph/0611084)
Pointecouteau, E., Arnaud, M., & Pratt, G. W. 2005, A&A, 435, 1
Power, C., Navarro, J. F., Jenkins, A., Frenk, C. S., White, S. D. M., Springel, V., Stadel, J., & Quinn, T. 2003, MNRAS, 338, 14
Pratt, G. W., & Arnaud, M. 2005, A&A, 429, 791
Rahman, N., Krywult, J., Motl, P. M., Flin, P., & Shandarin, S. F. 2006, MNRAS, 367, 838
Reed, D., Governato, F., Quinn, T., Gardner, J., Stadel, J., & Lake, G. 2005a, MNRAS, 359, 1537
Reed, D., Governato, F., Verde, L., Gardner, J., Quinn, T., Stadel, J., Merritt, D., & Lake, G. 2005b, MNRAS, 357, 82
Reid, B. A., & Spergel, D. N. 2006, ApJ, 651, 643
Reiprich, T. H., & Böhringer, H. 2002, ApJ, 567, 716
Ricotti, M. 2003, MNRAS, 344, 1237
Rines, K., & Diaferio, A. 2006, AJ, 132, 1275
Romeo, A. D., Sommer-Larsen, J., Portinari, L., & Antonuccio-Delogu, V. 2006, MNRAS, 371, 548
Ruhl, J., et al. 2004, Proc. SPIE, 5498, 11
Saha, P., Read, J. I., & Williams, L. L. R. 2006, ApJ, 652, L5
Salvador-Solé, E., Manrique, A., & Solanes, J. M. 2005, MNRAS, 358, 901
Scannapieco, E., & Oh, S. P. 2004, ApJ, 608, 62
Schmidt, R. W., & Allen, S. W. 2006, MNRAS, submitted (astro-ph/0610038)
Sealfon, C., Verde, L., & Jimenez, R. 2006, ApJ, 649, 118
Sehgal, N., Trac, H., Huffenberger, K., & Bode, P. 2007, ApJ, in press (astro-ph/0612140)
Shaw, L. D., Weller, J., Ostriker, J. P., & Bode, P. 2006, ApJ, 646, 815
Shimizu, M., Kitayama, T., Sasaki, S., & Suto, Y. 2004, PASJ, 56, 1
Sijacki, D., & Springel, V. 2006, MNRAS, 366, 397
Solanes, J. M., Manrique, A., González-Casado, G., & Salvador-Solé, E. 2005, ApJ, 628, 45
Spergel, D. N., et al. 2007, ApJS, in press (astro-ph/0603449)
Subramanian, K., Cen, R., & Ostriker, J. P. 2000, ApJ, 538, 528
Suto, Y., Sasaki, S., & Makino, N. 1998, ApJ, 509, 544
Tasitsiomi, A., Kravtsov, A. V., Gottlöber, S., & Klypin, A. A. 2004, ApJ, 607, 125
Tozzi, P., & Norman, C. 2001, ApJ, 546, 63
Verde, L., Haiman, Z., & Spergel, D. N. 2002, ApJ, 581, 5
Vikhlinin, A. 2006, ApJ, 640, 710
Vikhlinin, A., Kravtsov, A., Forman, W., Jones, C., Markevitch, M., Murray, S. S., & Van Speybroeck, L. 2006, ApJ, 640, 691
Voevodkin, A., & Vikhlinin, A. 2004, ApJ, 601, 610
Voit, G. M., & Bryan, G. L. 2001, ApJ, 551, L139
Voit, G. M., Bryan, G. L., Balogh, M. L., & Bower, R. G. 2002, ApJ, 576, 601
Wang, Y.-G., & Fan, Z.-H. 2006, ApJ, 643, 630
Warren, M. S., Abazajian, K., Holz, D. E., & Teodoro, L. 2006, ApJ, 646, 881

Wechsler, R. H., Bullock, J. S., Primack, J. R., Kravtsov, A. V., & Dekel, A. 2002, ApJ, 568, 52
Wechsler, R. H., Zentner, A. R., Bullock, J. S., Kravtsov, A. V., & Allgood, B. 2006, ApJ, 652, 71
Weller, J., Battye, R. A., & Kneissl, R. 2002, Phys. Rev. Lett., 88, 231301
White, M., Hernquist, L., & Springel, V. 2002, ApJ, 579, 16
Wu, K. K. S., Fabian, A. C., & Nulsen, P. E. J. 2000, MNRAS, 318, 889
Younger, J. D., Haiman, Z., Bryan, G. L., & Wang, S. 2006, ApJ, 653, 27
Zaldarriaga, M., & Seljak, U. 2000, ApJS, 129, 431
Zekser, K. C., et al. A. 2006, ApJ, 640, 639
Zhao, D. H., Jing, Y. P., Mo, H. J., & Börner, G. 2003, ApJ, 597, L9